Energy Storage Materials 72 (2024) 103758

Contents lists available at ScienceDirect

Energy Storage Materials

journal homepage: www.elsevier.com/locate/ensm

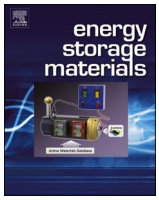

Wide electrochemical stability window of $NaClO_4$ water-in-salt electrolyte elevates the supercapacitive performance of poly (3,4-ethylenedioxythiophene)

Plawan Kumar Jha [a,*], Sachin Kochrekar [a], Ashwini Jadhav [a], Robert Lassfolk [b], Mikko Salomäki [a], Ermei Mäkilä [c], Carita Kvarnström [a,1,*]

[a] Department of Chemistry, University of Turku, Henrikinkatu 2, 20500 Turku, Finland
[b] Faculty of Science and Engineering, Laboratory of Molecular Science and Engineering, Åbo Akademi University, Henrikinkatu 2, 20500 Turku Åbo, Finland
[c] Laboratory of Industrial Physics, Department of Physics and Astronomy, University of Turku, Turku FI-20014, Finland

ARTICLE INFO

Keywords:
Supercapacitor
PEDOT
Water-in-salt electrolyte
Sodium perchlorate
Wide electrochemical stability window

ABSTRACT

Water-in-salt electrolytes (WiSEs) have emerged as the primary preference in the domain of aqueous-based supercapacitors, thanks to their wide electrochemical stability window (ESW > 1.23 V). Here, we have chemically synthesized a unique lettuce coral-like structure of tosylate doped-poly(3,4-ethylenedioxythiophene) (PEDOT-tos) and tested it for supercapacitor application in a 17 molal (m) $NaClO_4$ WiSE, achieving an ESW of 1.9 V. The energy and power densities (E_d and P_d) of our PEDOT-tos supercapacitor are as high as 14 Wh kg^{-1} and 7210 W kg^{-1}, respectively, with over 80 % capacitance retention after 10,000 continuous Galvanostatic charge-discharge cycles. The $NaClO_4$ WiSE increases the E_d and P_d of PEDOT by several folds compared to traditional H_2SO_4 electrolyte. This work encourages the exploration of a suitable combination of a PEDOT-based composite material and WiSE for high-performance supercapacitors.

1. Introduction

A wide electrochemical stability window (ESW) is essential for a supercapacitor device (SC), and it is mostly governed by two major components – electrode active material and electrolyte [1-4]. Non-aqueous systems, such as organic electrolytes and ionic liquids, have been considered electrolytes with a wider ESW and are used for practical SC applications for decades, despite their several associated problems, such as high cost and flammability [4,5]. The aqueous electrolytes, on the other hand, are well-established for laboratory-scale research. However, they have been considered unsuitable for practical SC applications due to their limited ESW of 1.23 V [3]. Even so, continuous research on widening the ESW of aqueous electrolytes demonstrated its significance both in batteries and supercapacitors [3,5]. In 2015, Suo et al. have successfully expanded the ESW of highly concentrated aqueous lithium bis(trifluoromethane sulfonyl)imide (LiTFSI) electrolyte to ~3 V, introducing the concept of water-in-salt electrolyte (WiSE) [6]. A WiSE is characterized by high salt-to-water ratio in a highly concentrated aqueous electrolyte [6-8]. Furthermore, it was observed that the formation of an aqueous solid-electrolyte interphase (SEI) at the anode electrode increased the thermodynamic stability limit of water [6,7]. The insightful studies by Suo et al. have provided a molecular-level understanding of the processes involved during aqueous SEI formation [9]. The electrochemical reaction between water molecules, electrolyte anions, and dissolved gases (such as O_2 and CO_2) at the electrode-electrolyte interface produces an electrically insulating SEI, which typically facilitates the diffusion of electrolyte ions and prevents the decomposition of electrolytes up to a certain potential [9]. The significance of WiSE has been extensively explored, resulting in the introduction of numerous WiSE in batteries, supercapacitors, and other energy research, such as LiTFSI [6], $LiClO_4$ [10], $NaNO_3$ [10], $NaCF_3SO_3$ [11], CH_3COOK [12], NaOTF-TEAOTF [13], Li_2SO_4 [14], and $NaClO_4$ [15]. So far, they have shown great potential in battery research and made their mark in the field of supercapacitors. Noticeably, the importance of selecting the specific WiSE for a particular set of materials has been recognized as crucial in achieving high performance in energy storage devices [15]. Moreover, $KTi_2(PO_4)_3$ [12] and $NaTiOPO_4$ [13] anodes of a battery showed elevated performance in

* Corresponding authors.
E-mail addresses: plawanjha@gmail.com (P.K. Jha), carkva@utu.fi (C. Kvarnström).
[1] Lead Contact.

https://doi.org/10.1016/j.ensm.2024.103758
Received 29 March 2024; Received in revised form 30 June 2024; Accepted 31 August 2024
Available online 1 September 2024
2405-8297/© 2024 The Authors. Published by Elsevier B.V. This is an open access article under the CC BY-NC-ND license (http://creativecommons.org/licenses/by-nc-nd/4.0/).

CH_3COOK and NaOTF-TEAOTF WiSEs, respectively, whereas, SWNT [16] and Ketjen black [17] based supercapacitor showed high performance in $NaClO_4$–NaBr–$CcPF_6$ and $NaClO_4$ WiSEs, respectively. Recently, M. H. Lee et al. compared different salt-based electrolytes and emphasized the significance of employing Na^+-based WiSEs because of their low cost and high ionic conductivity [15]. Various materials have demonstrated improved supercapacitive performance in a $NaClO_4$ WiSE, for example carbonaceous materials and metal oxides, mainly because of the wide ESW and suitable ion percolations [8,14,16,17]. However, there are several well-known materials that need to be investigated in the WiSEs for better supercapacitor performance. In the domain of polymers, poly(3,4-ethylenedioxythiophene) (PEDOT) is renowned and widely employed in the field of energy storage, optoelectronics, sensors, transducers, and solar cells, due to its easy synthesis, processability, low cost, conjugation, high conductivity, absence of chemical defects, long term environmental stability, and biocompatibility [18-21]. The supercapacitive performance of PEDOT-based materials in aqueous H_2SO_4 [22-25], Na_2SO_4 [26], HCl [20], KOH [27], $LiClO_4$ [28], NaCl [29], and even artificial sweat [30] is widely evaluated, however their performance in WiSE is unexplored. Nonetheless, H_2SO_4 electrolyte was often the primary choice for aqueous-based PEDOT supercapacitor due to its high ionic conductivity and percolation. Apart from the electrolytes, morphology and counterion are crucial parameters which could significantly affect the supercapacitive performance of PEDOT. These parameters could be controlled during the synthesis of PEDOT [31-34]. PEDOT can be synthesised in bulk by a simple chemical approach or can be grown directly on a conducting or non-conducting substrate using methods such as electrochemical polymerisation, oxidative chemical vapour deposition (oCVD), vacuum vapor phase polymerisation (VVPP), and vapor phase polymerization (VVP) [19,21].

Here, tosylate doped–PEDOT (here after PEDOT-tos) is chemically synthesized in bulk by an oxidative polymerization approach using iron (III) p-toluenesulfonate hexahydrate (Fe(III) tosylate) and 3,4-Ethylenedioxythiophene (EDOT) compounds. Spectroscopic and microscopic tools were employed to monitor the formation of PEDOT-tos. The high conductivity and lettuce coral-like structure made it a suitable candidate for supercapacitor application. The PEDOT-tos slurry (loading = 2 mg cm^{-2}) was drop-casted on graphite sheets, dried, and pressed under high pressure (~0.5 ton) before electrochemical characterization in 1 M H_2SO_4, 1 m (m = mol kg^{-1}) and 17 m $NaClO_4$ electrolytes. We achieved a 1.9 V and 2.2 V ESW in 17 m $NaClO_4$ WiSE compared to 1.6 V and 1 V ESW in 1 m $NaClO_4$ and 1 M H_2SO_4 electrolytes, respectively, which to the best of our knowledge, is the widest potential window achieved for a PEDOT in an aqueous electrolytic system (Tables S1 and S2). The high capacitance (110 F g^{-1}) and increased ESW (1.9 V) significantly improved the energy (14 Wh kg^{-1}) and power (7210 W kg^{-1}) densities of PEDOT-tos supercapacitor. Our results encourage the use of WiSE in conducting polymer-based systems for improved supercapacitive performance.

2. Experimental section

2.1. Materials

3,4-Ethylenedioxythiophene (EDOT, >98 %) and N-Methyl-2-pyrrolidone (NMP, >99 %) were purchased from TCI chemicals. Iron(III) p-toluenesulfonate hexahydrate (Fe(III) tosylate, technical grade) and sulfuric acid (H_2SO_4, 1 M) were purchased from Merck. Sodium perchlorate anhydrous ($NaClO_4$, ACS reagent ≥98 %) was purchased from Thermo scientific. Ethanol (70 %) was purchased from VWR chemicals BDH®. TIMCAL super P conducting carbon black was purchased from Nanografi Nano Technology. The 5 % Nafion 117 solution in water and alcohol was purchased from Aldrich.

2.2. Material preparation

Fe(III) tosylate, about 8.42 g, was dissolved in 50 mL double distilled water (DI water) in a 100 mL round bottom flask, and stirred at 50 °C for 15 min. Subsequently 0.688 mL EDOT was injected into the solution and the reaction was continued for next 18 h at 50 °C. The final dark colored product was washed with DI water and ethanol and dried in a vacuum oven at 70 °C for 12 h.

2.3. Materials characterization

PEDOT-tos was characterized by Raman spectroscopy (Renishaw inVia confocal Raman microscope, 532 nm diode laser), UV–visible spectroscopy (UV–vis; Cary 60 spectrophotometer, Agilent), Fourier-transform infrared spectroscopy (FTIR; Bruker Vertex70), powder X-ray diffraction (PXRD; PANalytical Aeris with Cu Kα = 1.564 Å), thermogravimetric analysis (TGA; under N_2, TA Instruments Q600 SDT), field emission scanning electron microscopy (FE-SEM; Thermo Scientific Apreo S), transmission electron microscopy (TEM; JEOL JEM-2200FS), and X-ray photoelectron spectroscopy (XPS; Thermo Scientific Nexsa XPS with a monochromatized Al K_α = 1486.7 eV source). XPS was performed under a base vacuum of ~10^{-9} mbar. Four-probe current-voltage measurements were performed on a pressed pellet (5 ton) (I-V; Keithley 2460 source meter). The ^{17}O NMR spectra were recorded using a Bruker Avance-III spectrometer operating at 500.20 MHz (^1H) and 67.81 MHz (^{17}O) equipped with a Smartprobe: BB/1H. The spectra were recorded at 298 K using a standard zg pulse sequence with a recycle delay of 0.10 s and the number of scans set to 5120. The ^{23}Na NMR spectra were recorded using a Bruker Avance-III spectrometer operating at 500.20 MHz (^1H) and 132.31 MHz (^{23}Na) equipped with a Prodigy BBO CryoProbe. The spectra were recorded at 298 K using a standard zg30 pulse sequence with a recycle delay of 2.00 s and the number of scans set to 64. Density (at ~25 °C), viscosity (at ~25 °C), and conductivity (at ~25 °C) of electrolytes were measured on digital density meter AP Paar DMA45, automated micro viscometer Anton Paar DMVn, and Orion conductivity meter model 150, respectively. The N_2 adsorption-desorption isotherm was determined using 3Flex 3500 analyzer (Micromeritics Corp., Norcross, GA, USA) and the SSA was calculated with the Brunauer-Emmett-Teller (BET) method using MicroActive v5.01 software (Micromeritics Corp.).

2.4. Electrochemical characterization

The ink for active electrodes was prepared by mixing 80 wt% PEDOT-tos, 10 wt% carbon, 10 wt% Nafion solution, and 0.3 mL NMP in a mortar pestle. The ink was dropcasted on a graphite sheet and dried in oven at 80 °C for 10 h. The electrodes were pressed under high pressure (~0.5 ton) before electrochemical characterization (Fig. S5). Total loading of the material (active material (1.6 mg) + carbon (0.2 mg) + nafion (0.2 mg)) on each electrode was about 2 mg cm^{-2}. In a 3-electrode setup, Ag/AgCl and graphite sheet were used as a reference and counter electrodes, respectively. For a supercapacitor, all electrochemical characterizations were performed in a symmetric 2-electrode setup in 1 M H_2SO_4, 1 m $NaClO_4$, and 17 m $NaClO_4$ electrolyte solutions using Iviumstat (IVIUM) and BioLogic VSP-300 Galvanostat/Potentiostat workstations.

3. Results and discussion

In a typical synthesis of PEDOT-tos, EDOT is mixed with aqueous Fe (III) tosylate and heated at 50 °C for 18 h (Fig. 1a). Time-dependent studies were carried out to monitor the formation and growth of PEDOT-tos (Fig. 1b-d). Raman (Fig. 1b) and UV–vis (Fig. 1c) spectra showed the characteristic peaks of PEDOT appearing within 1 min of EDOT addition, however, extra hours were required to form a network structure of PEDOT-tos as can be seen in Fig. 1d. In Raman spectroscopy,

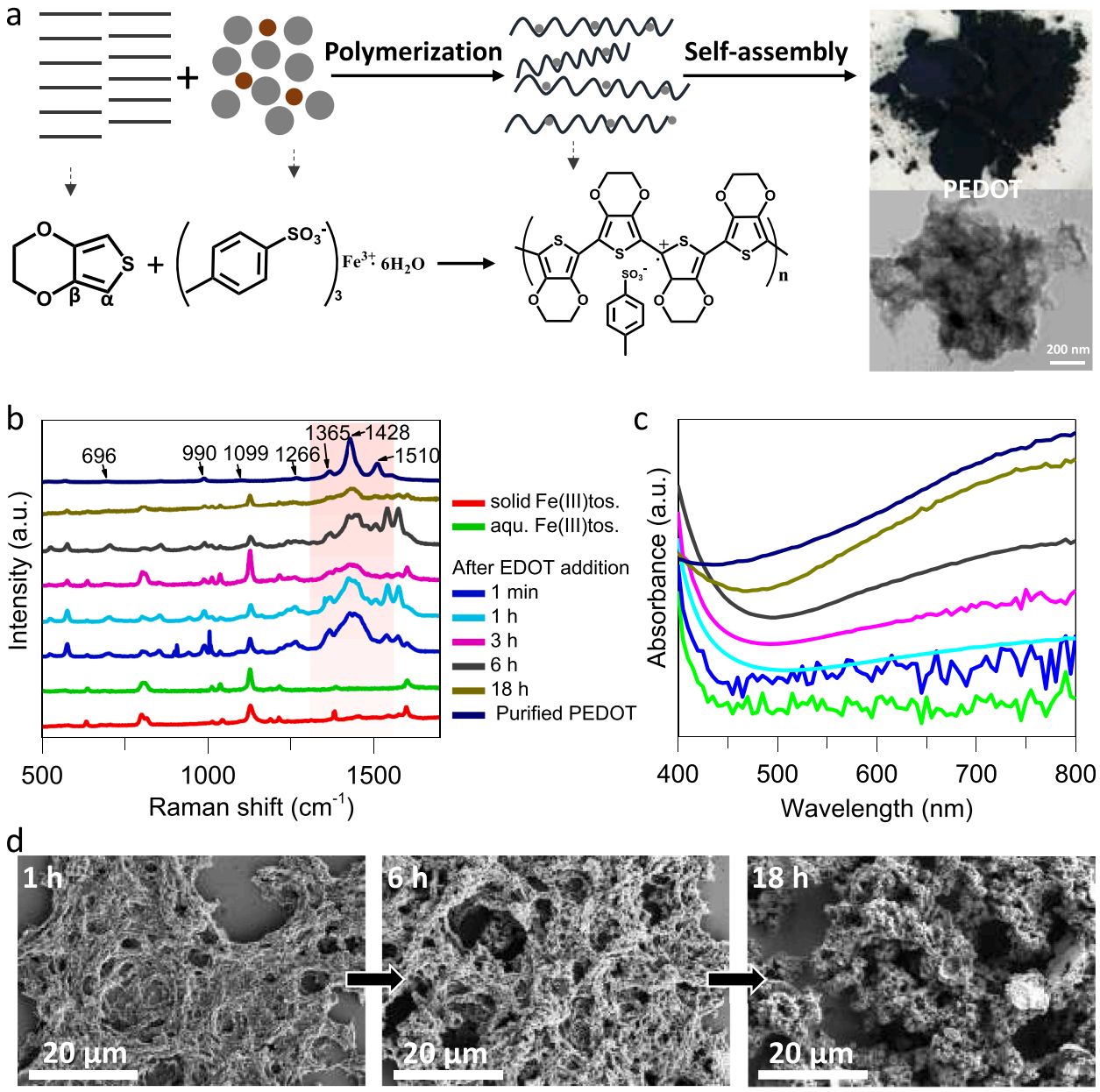

Fig. 1. (a) Left panel: schematic of the synthesis process of PEDOT-tos via oxidative polymerization of EDOT by Fe(III) oxidant and their structures (dark orange sphere: Fe(III) and dark grey sphere: tosylate); Right panel: purified PEDOT-tos powder (top) and its morphology (bottom, TEM image), (b-c) Time dependent Raman and UV–vis spectroscopy plots of PEDOT-tos synthesis, and (d) SEM images of PEDOT-tos at different time interval (1, 6, and 18 h) of the reaction.

after 1 min of the reaction, a symmetric stretching peak of $C_\alpha{=}C_\beta(-O)$ appeared around 1422 cm^{-1} and later shifted to 1428 cm^{-1}, indicating a high-level doping of tosylate anion in PEDOT [35]. We expected high doping-efficiency in PEDOT because of the small size and single negative charge of the dopant ion. Other stretching modes of PEDOT, such as symmetric C–S–C deformations, oxyethylene ring deformation, C–O–C deformation, C_α–$C_{\alpha'}$ inter-ring, C_β–$C_{\beta'}$, and asymmetric $C_\alpha{=}C_\beta$, appeared at 696, 990, 1099, 1266, 1365, and 1510, respectively, confirmed the formation of PEDOT (Fig. 1b) [18,35]. The intermolecular C—C bond can provide the conjugation pathways for easy charge transport along the polymer chain of PEDOT. The UV–vis measurement showed a continuously increasing broad band absorbance in the 500–800 nm region (due to the π–π* transition) as the reaction progressed [20]. The gradual enhancement of the absorbance band of PEDOT-tos suggested the formation of a conductive metallic state due to substantial doping by the tosylate anion (Fig. 1c) [18]. This time- dependent growth study suggested that the formation of polymer networks of PEDOT-tos took place after 1 h of the continuous polymerization reaction. In 18 h of reaction time, these polymer networks expanded in all three dimensions, probably by a self-assembly process. This resulted in a porous lettuce coral-like network of PEDOT-tos (Fig. 1d). Further, SEM and TEM images revealed the thin sheets of PEDOT-tos interconnected into a porous lettuce coral-like structure with numerous channels (Fig. 2a– c and S1), which are crucial for facile ions percolation during electrochemical testing for supercapacitors. In the PXRD (Fig. S2a), peaks appearing at scattering angles $2\theta = 6.5°$, 12.7°, and 26.3° were assigned to the (100), (200), and (020) planes, respectively [36]. Furthermore, both planes at lower scattering angles were attributed to the lateral chain packing of PEDOT-tos, whereas the plane at higher angle indicated the π–π stacking of the polymer chains [20].

The fitted O 1s and S 2p XPS spectra are shown in Fig. 2d and 2e, respectively. The corresponding peaks of dioxane ring (C—O–C) of PEDOT and O–S of tosylate appeared at around 532.8 eV and 530.4 eV binding energies, respectively (Fig. 2d) [37]. The S 2p XPS showed two

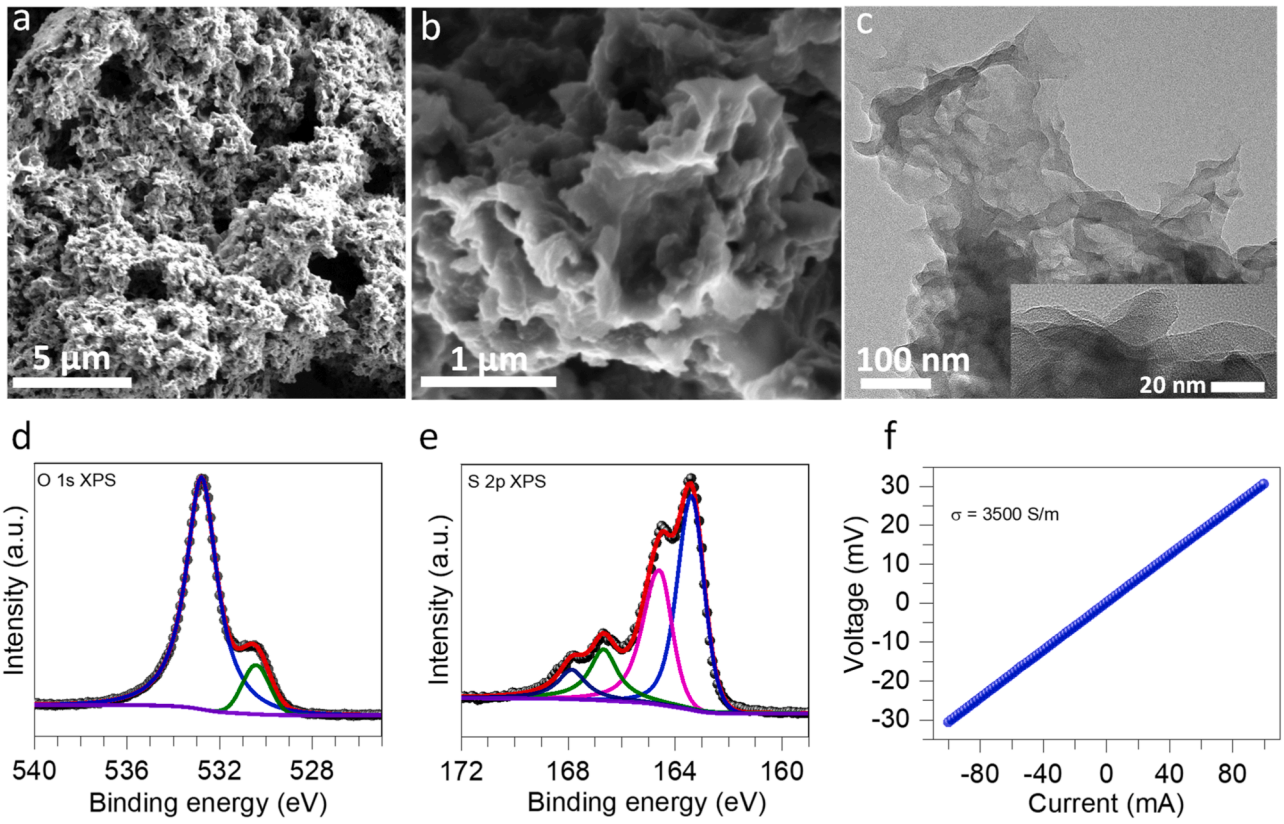

Fig. 2. (a-b) SEM images of PEDOT-tos, (c) TEM image of PEDOT-tos, inset: high-resolution image, (d-e) O 1s and S 2p XPS of PEDOT-tos, and (f) Four-probe current-voltage (I-V) plot of PEDOT-tos.

doublets due to two different chemical environments of sulfur. The S $2p_{3/2}$ peaks at 163.4 eV and 166.7 eV binding energies were assigned to the thiophene of PEDOT and $-SO_3^-$ of tosylate, respectively (Fig. 2e) [37]. The characteristic XPS peaks of undoped PEDOT [37], unbound tosylates, and Fe(III)/(II) (Fig. 2d, e, and S3) were not observed. Our PEDOT-tos showed very high conductivity (σ = 3500 S m^{-1}) which is mainly due to the fine conjugated polymer networks and sufficient tosylate doping (Fig. 2f). Apart from doping, tosylate may have played a significant role in shaping the unique structure during the polymerization and self-assembly processes of PEDOT-tos. A detailed mechanistic study could reveal the roles of tosylate and temperature in the formation of the unique lettuce coral-like network of PEDOT-tos. Our PEDOT-tos showed good thermal stability up to 300 °C with only 5 % weight loss (Fig. S2b). N_2 gas adsorption-desorption isotherms at 77 K showed characteristic of a type-II isotherm (Fig. S4a). The BET surface area and pore diameter were 40 m^2/g and 1.3 nm, respectively (Fig. S4b).

The performance of a supercapacitor is not only influenced by various properties of a material but also readily affected by three crucial parameters of an electrolyte – density (d), viscosity (η), and conductivity (σ). We observed that the values of these parameters increased as the concentration of $NaClO_4$ was increased from 1 m to 17 m. For 1 m $NaClO_4$ solution, the d, η, and σ were 1.074 g cm^{-3}, 0.931 mPa.s, and 83.0 mS cm^{-1}, respectively, whereas, for 17 m $NaClO_4$ solution these increased to 1.664 g cm^{-3}, 6.168 mPa.s, and 122.8 mS cm^{-1}, respectively (Fig. 3a). The d and η of 1 M H_2SO_4 were around 1.054 g cm^{-3} and 1.068 mPa.s, respectively, while the σ value of 1 M H_2SO_4 is reported to be around 250 mS cm^{-1} [38]. Previously, the unique solvation chemistry of aqueous and nonaqueous solutions of $NaClO_4$ was well-studied using Raman and NMR spectroscopic techniques [15,39-41]. These studies have explained the formation of contact ion pairs (CIP) and ^{23}Na NMR chemical shifts in the solutions [39,40]. Here, we have employed the same spectroscopic techniques (Fig. 3b– e) for 1 m and 17 m $NaClO_4$ solutions and the outcomes were compared with the previous findings. For solid $NaClO_4$ salt, a narrow Raman peak centered at 953.3 cm^{-1} is assigned to the perchlorate (Fig. 3b) [42]. In the case of 1 m $NaClO_4$ solution, a slightly broadened peak centered at 935.3 cm^{-1} is assigned to stretching vibration $v_1(A_1)$ of dissociated ClO_4^- ion (Fig. 3b) [39]. It also suggested that most ions are in the form of free anions (FA) and solvent-separated ion pairs (SSIP). For 17 m $NaClO_4$ solution, a broader vibration peak appeared around 940.5 cm^{-1} (Fig. 3b). The significant blue shift (5.2 cm^{-1}) from dilute to concentrated solution is ascribed to the transition of the FA and SSIP into the CIP [15,39]. In 17 m $NaClO_4$ solution, the ClO_4^- ions can break the hydrogen bonding networks of water and form different electrolytic ions network. Double distilled (DI) water did not show any peak in this region. The effect of salt concentration on the hydrogen bonding networks of water was realised by following Raman shift of O—H stretching envelope of water molecules [15,43]. In Fig. 3c, DI water showed a broad spectrum with two strong bands at around 3229 cm^{-1} and 3423 cm^{-1} and a weak band at around 3632 cm^{-1} [43]. The strong bands attributed to the strong hydrogen bonding between water molecules, originated from the ice-like component and ice-like liquids, and the weak band at higher frequency was assigned to monomeric water molecules (Fig. 3c) [43]. For the 1 m solution, an additional weak shoulder at around 3554 cm^{-1} was due to the Na^+–coordinated water molecules [15,43]. The disappearance of the bands at lower frequency and the appearance of a sharp peak at 3554 cm^{-1} suggested the formation of crystalline hydrates, where most of the water molecules are engaged/coordinated with the Na^+ and ClO_4^- ions (Fig. 3c) [43]. The high solute-to-water ratio in the 17 m $NaClO_4$ solution significantly reduces the hydrogen bonding among water molecules, preventing independent water activities. Furthermore, we have recorded ^{17}O and ^{23}Na NMR spectra of 1 m and 17 m $NaClO_4$ solutions (Fig. 3d, e). We expect the chemical shift to change in both cases due to the different electronic densities around Na^+ and ClO_4^- ions in 1 m and

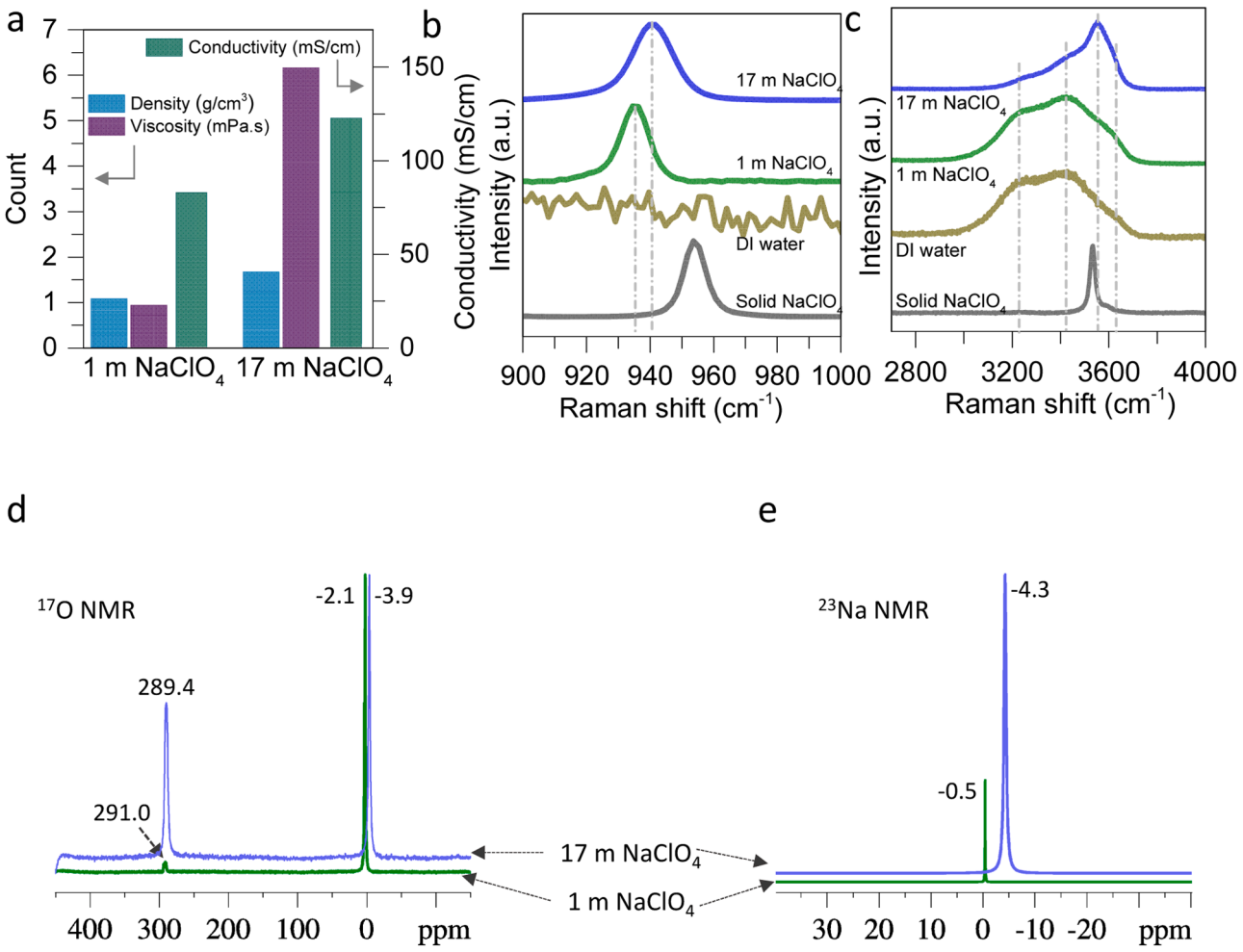

Fig. 3. (a) Density, viscosity, and conductivity of 1 m and 17 m $NaClO_4$ solutions at 25 °C, (b-c) Raman spectra of solid $NaClO_4$, DI water, 1 m $NaClO_4$, and 17 m $NaClO_4$ solutions, and (d-e) ^{17}O and ^{23}Na NMR spectra of 1 m and 17 m $NaClO_4$ solutions.

17 m solutions. Fig. 3d displayed the chemical shifts in ^{17}O NMR spectra of 1 m and 17 m $NaClO_4$ solutions. For 1 m $NaClO_4$ solution, the peaks of H_2O and ClO_4^- appeared at around −2.1 ppm and 291.0 ppm, respectively. These peaks upshifted to −3.9 ppm and 289.4 ppm, when the concentration of $NaClO_4$ was increased to 17 m (Fig. 3d). In ^{23}Na NMR, a similar chemical shift was observed with an increased concentration of $NaClO_4$ salt (Fig. 3e). Our results of this unique solvation chemistry of electrolytic ions are in accord with the previous literatures [13,40].

The cyclic voltammetry (CV) characterization in a 3-electrode setup was performed to determine the ESW in 1 M H_2SO_4, 1 m $NaClO_4$, and 17 m $NaClO_4$ electrolytes (Fig. 4a). In 1 M H_2SO_4 and 1 m $NaClO_4$ electrolytes, an electrolytic oxidation–reduction was observed beyond −0.15 to 0.85 V and −0.8 to 0.8 V potentials, respectively. In the 17 m $NaClO_4$ electrolyte, electrolytic oxidation was observed above 0.95 V anodic potential, whereas the electrode showed resistance below −0.95 V potential. In some literature reports, the selection of ESW was based on the electrochemical activity of the material in the WiSE [17,42]. Here, we have restricted the ESW to 1 V, 1.6 V, and 1.9 V for the supercapacitive testing of PEDOT-tos in 1 M H_2SO_4, 1 m $NaClO_4$, 17 m $NaClO_4$ electrolytes, respectively. Electrochemical characterization of a symmetric PEDOT-tos supercapacitor in 1 M H_2SO_4, 1 m $NaClO_4$, and 17 m $NaClO_4$ electrolytes was performed using CV (scan rate (ν) = 5–500 mVolt/*sec* (mV s^{-1})), Galvanostatic charge-discharge (GCD, current density (J) = 0.25–20 Ampere/gram (A g^{-1})), and electrochemical impedance spectroscopy (EIS, frequency = 1 MHz – 1 mHz; 20 mV constant potential) techniques. The rectangular nature of the CV curve of PEDOT-tos supercapacitors in all three electrolytes, indicated the charge storage mainly via electric double-layer (EDL) formation at the electrode-electrolyte interface (Fig. 4b) [1,44]. The rectangular nature of the curves throughout the scan rates up to 500 mV s^{-1} suggested the good rate-stability of our material (Fig. S6a, c, e) [1,44]. The ESW of PEDOT-tos supercapacitor in aqueous acidic electrolyte is 1 V (Fig. 4b). Interestingly, PEDOT-tos supercapacitor showed excellent stability in 1 m and 17 m $NaClO_4$ electrolyte solutions by maintaining its EDLC nature beyond 1 V (potential > 1 V, Fig. 4b). Stability of PEDOT-tos to such a range of potentials signified the robustness of polymer backbone and suggested the right choice of WiSE to begin with. We have achieved high ESW values of 1.6 V and 1.9 V in 1 m and 17 m $NaClO_4$ electrolytes, respectively (Fig. 4b). To the best of our knowledge, ESW = 1.9 V is the highest value for any symmetric PEDOT-tos supercapacitor in any aqueous electrolytic solution (Table S1). Achieving high ESW for a supercapacitor is crucial to the elevate energy density ($E \alpha ESW^2$). In order to understand the state of polymer backbone and doping-level we have performed ex-situ Raman spectroscopy on PEDOT-tos electrodes at 0, 0.5, 1, 1.5, and 1.9 V potentials. Firstly, we have performed multiple CV scans at a $\nu = 50$ mV s^{-1} prior to Raman measurement. After that, we halted the forward CV scan at each aforementioned potential (Fig. 4c), and measured Raman spectra (Fig. 4d). At 0 V, the symmetric $C_\alpha{=}C_\beta(-O)$ stretching peak of the unused PEDOT-tos electrode (1430 cm^{-1}) red-shifted to 1442 cm^{-1}, indicating the slight enhancement of doping-level during the initial CV scans [35]. This peak underwent a red-shift at each higher potential and ultimately reached to 1455 cm^{-1} at 1.9 V potential, suggesting the high-level doping of PEDOT-tos [35]. Moreover, PEDOT-tos regained its initial doping state (1438 cm^{-1}) when

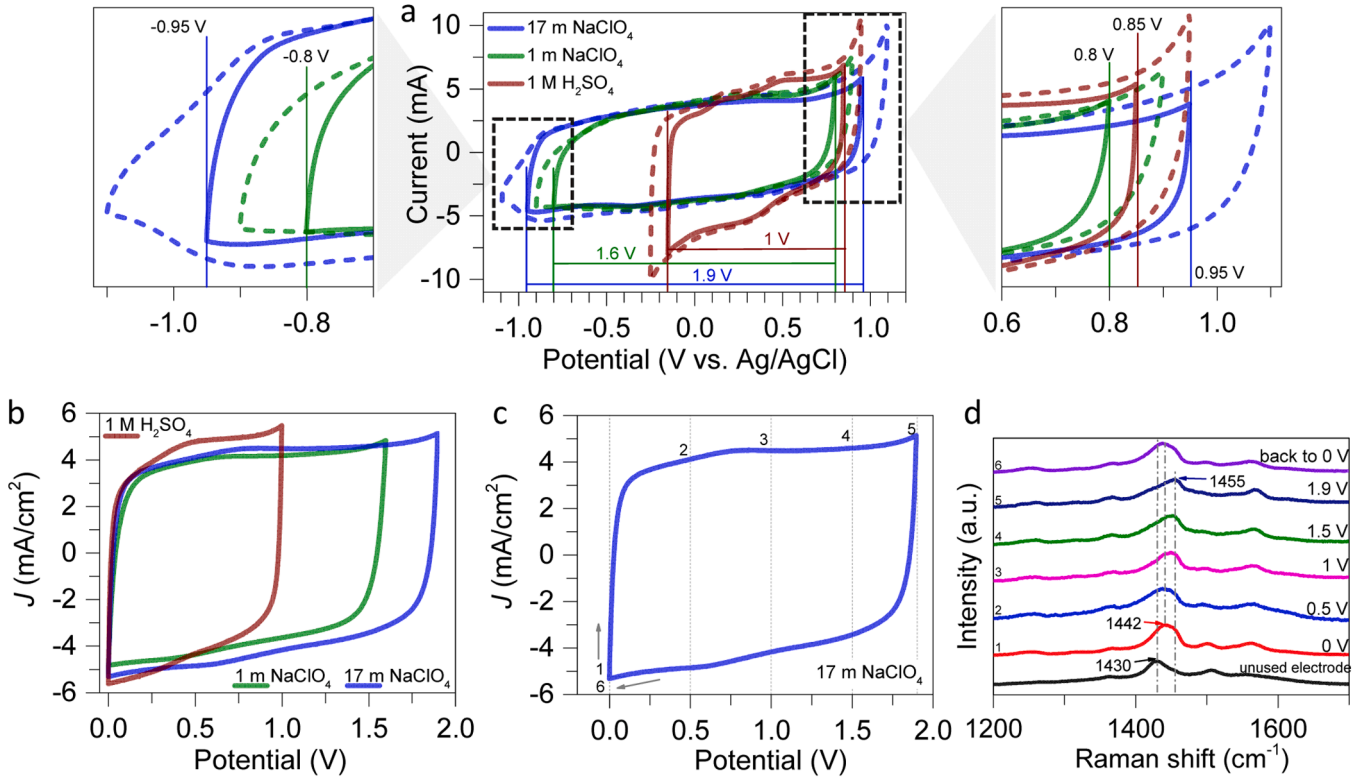

Fig. 4. (a) CV ($v = 20$ mV s^{-1}) plots of PEDOT-tos in 1 M H_2SO_4, 1 m $NaClO_4$, and 17 m $NaClO_4$ electrolytes; determination of stable potential window of the materials in the respective electrolytes. Left and right panels are the zoomed-in graphs, (b) CV plots of PEDOT-tos supercapacitors in 1 M H_2SO_4, 1 m $NaClO_4$, and 17 m $NaClO_4$ electrolytes ($v = 50$ mV s^{-1}), (c) CV plot of PEDOT supercapacitor in 17 m $NaClO_4$ WiSE ($v = 50$ mV s^{-1}) (dotted lines in the CV denote the potentials at which the scan was held before Raman measurements), and (d) Ex-situ Raman spectra of PEDOT-tos electrode at different potentials.

the potential was reversed back to 0 V (Fig. 4d). This suggested that PEDOT-tos could store charge in a reversible fashion without any serious impairment within a wide ESW of 1.9 V.

In GCD measurement, the triangular nature of the curves of PEDOT-tos supercapacitor in all three electrolytes corroborated with CV (Fig. 5a and S6b, d, f). Furthermore, PEDOT-tos supercapacitor exhibited higher discharge time at each applied current density ($J = 0.25 – 20$ A g^{-1}) in 17 m $NaClO_4$ electrolyte solution compared to 1 M H_2SO_4 and 1 m $NaClO_4$ electrolytes, which is due to the wide ESW of WiSE (Fig. 5a and S6b, d, f). Using formulae S1 and S2, we have calculated the gravimetric capacitance ($C_{gr.}$ per electrode) of PEDOT-tos supercapacitor and plotted against J (Fig. 5b). PEDOT-tos showed $C_{gr.}$ value of around 132 F g^{-1} (at $J = 0.25$ A g^{-1}) in 1 M H_2SO_4, which is noteworthy. On the other hand, the $C_{gr.}$ value of PEDOT-tos in 1 m and 17 m $NaClO_4$ electrolytes was calculated to be around 99 F g^{-1} and 112 F g^{-1} (at $J = 0.25$ A g^{-1}), respectively (Fig. 5b). It is interesting to note here that the capacitance values of PEDOT-tos in H_2SO_4 and WiSE are close. Due to the superior ionic conductivity of protons, aqueous acidic electrolytes are the preferred choice for standard supercapacitance measurements. Although the use of WiSE sometimes comes at the cost of capacitance value, the enhancement of ESW (most of the time) increases the energy density of the supercapacitor. Here, we not only achieved an ESW of 1.9 V but also obtained a high capacitance value. High-rate stability of a supercapacitor is crucial for constant delivery of capacitance at various current densities. Here, in all three electrolytes, PEDOT-tos supercapacitor showed >60 % rate stability even at a high current density of 20 A g^{-1} (Fig. 5b). This indicates the facile access of pores in PEDOT-tos by the electrolyte ions (Fig. 5b). The rate-independent capacitance values of PEDOT-tos supercapacitor in 1 M H_2SO_4, 1 m $NaClO_4$, and 17 m $NaClO_4$ electrolytes were around 87 F g^{-1}, 73 F g^{-1}, and 79 F g^{-1}, respectively (Fig. 5c and equation S5). Since the capacitance values of PEDOT-tos in acidic and $NaClO_4$ electrolytes were close, we also expected a similar trend for the rate-independent capacitance values. The Nyquist and Bode phase plots of PEDOT-tos supercapacitor were extracted from the EIS measurement. The equivalent series resistance (ESR) in 1 M H_2SO_4, 1 m $NaClO_4$, and 17 m $NaClO_4$ electrolytes were 2.0 Ω, 7.0 Ω, and 3.7 Ω, respectively (Fig. 5d). Similarly, the time constant (τ_o) was different in different electrolytes. The τ_o (and Bode phase angle (φ) at 10 mHz) [45] of PEDOT-tos supercapacitor in 1 M H_2SO_4, 1 m $NaClO_4$, and 17 m $NaClO_4$ were 1.42 s ($\varphi = -79.8°$), 5 s ($\varphi = -79.5°$), and 2.9 s ($\varphi = -80.1°$), respectively (Fig. 5e). Both ESR and τ_o of PEDOT-tos supercapacitor followed the trend 1 M H_2SO_4 < 17 m $NaClO_4$ < 1 m $NaClO_4$. This is mainly due to the ionic conductivity of the electrolytes, as the ease of ion percolation and de-percolation into the pores of the material during charging and discharging cycles, determines the value of ESR and τ_o of a supercapacitor [17,44]. Low ESR and τ_o in 1 M H_2SO_4 are mainly due to the high ionic conductivity of H^+. On the other hand, lower ESR and τ_o values in 17 m $NaClO_4$ electrolyte compared to 1 m $NaClO_4$ electrolyte are due to the higher ionic conductivity of Na^+ in the former compared to the latter (Fig. 3a). Furthermore, we have measured the self-discharge life of PEDOT supercapacitor in all three electrolytes (Fig. 5f). In 40 h of time span, PEDOT-tos supercapacitor slowly self-discharged up to 74 % and 84 % in 17 m $NaClO_4$ and 1 m $NaClO_4$ electrolytes, respectively (Fig. 5f). We observed a rapid self-discharge rate in 1 M H_2SO_4 electrolyte, where around 80 % discharge occurred only within 10 h (Fig. 5f). It is important to note here that the self-discharge tests were performed in an open condition, therefore, a small intervention by oxygen or other foreign substances cannot be avoided [46]. Notwithstanding, such steady charge storage capacity of PEDOT-tos supercapacitor in 17 m $NaClO_4$ signified the use of WiSE, where a side reaction originating due to impurities and oxygen could be easily suppressed.

The charge-storage process in a supercapacitor varies with materials and electrolytes, which are either dominated by surface capacitive

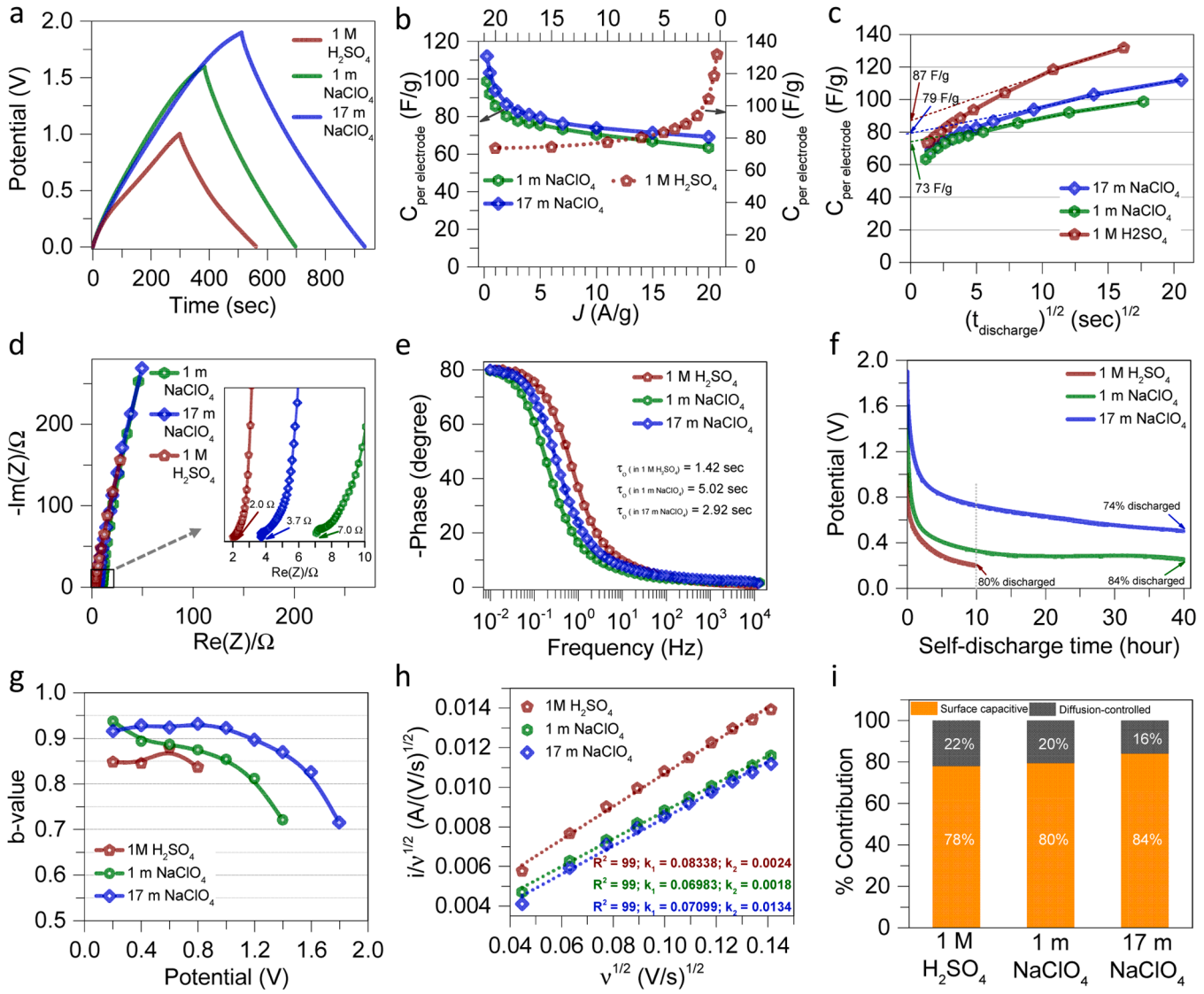

Fig. 5. (a) Galvanostatic charge-discharge, (b) Gravimetric capacitance versus current density, (c) rate independent capacitance, (d) Nyquist, (e) Bode phase, (f) Self-discharge, (g) b-value versus potential, (h) k_1 and k_2 determination, (i)% contribution of surface capacitance and diffusion-controlled processes at a potential and scan rate of 0.6 V and 10 mV s^{-1}, respectively, plots of PEDOT-tos supercapacitors in 1 M H_2SO_4, 1 m $NaClO_4$, and 17 m $NaClO_4$ electrolytes.

effects or diffusion-controlled processes [47-49]. The b-values of PEDOT-tos supercapacitor in all three electrolytes were determined using equation i (v) = av^b (equation1 (E1)) where i is current in A, v is scan rate in V s^{-1}, and a *and* b are variables (Fig. 5g, S7, S9, and S11) [48]. The b-values closer to 0.5 indicated diffusion-controlled processes and near 1 suggested surface capacitive effects [48]. Here, due to different ESW of electrolytes, the number of collected data points varied for PEDOT-tos supercapacitor (Fig. 5 g). The b-values were calculated from the anodic sweep of CVs (v = 2 to 20 mV s^{-1}) at 0.2, 0.4, 0.6, 0.8, 1.0, 1.2, 1.4, 1.6, and 1.8 V potentials (Fig. 5 g). PEDOT-tos supercapacitor showed a similar trend in each electrolyte where surface capacitive processes dominate the charge storage. Furthermore, the b-values decreased slowly at higher potentials and reached close to 0.7 at potentials near the ESW of 1 m and 17 m $NaClO_4$ electrolytes (Fig. 5 g). This indicated the dominated diffusion-controlled processes at the potentials closer to the ESW of the electrolytes. Percent contribution of diffusion-controlled (diff. cont.) and surface capacitive (surf. cap.) were calculated from CV plots (v = 2 to 20 mV s^{-1}) using the equation i (V) = $k_1v + k_2v^{1/2} = i_{\text{diff. cont.}} + i_{\text{surf. cap.}}$ (E2) (Fig. 5 h, i, S8, S10, and S12) [48]. At a potential of 0.6 V and scan rate of 10 mV s^{-1} PEDOT-tos supercapacitor showed 78 %, 80 %, and 84 % surface capacitive contribution in 1 M H_2SO_4, 1 m $NaClO_4$, and 17 m $NaClO_4$ electrolytes, respectively (Fig. 5i). Fig. S8, S10, and S12 clearly indicated that the % contribution of the surface capacitive process increased with increased scan rates. Moreover, surface capacitive effects were observed to be more dominant at the lower potentials, however, diffusion-controlled processes take over as soon as the potential reached close to the ESW of the electrolyte. These trends corroborate the b-values of PEDOT-tos supercapacitor in all three electrolytes.

The gravimetric energy (E_d) and power (P_d) densities of PEDOT-tos supercapacitor in all three electrolytes were calculated from GCD curves using formulae S3 and S4. The total weight of the coated material on both electrodes was considered during calculations. The maximum energy density ($E_{d.max.}$) and power density ($P_{d.max.}$) of PEDOT-tos in 1 M H_2SO_4 were around 4.5 Wh kg^{-1} and 3850 W kg^{-1}, respectively Fig. 6a). Whereas, in 1 m $NaClO_4$ these values increased to 8.6 Wh kg^{-1} ($E_{d.max.}$) and 4100 W kg^{-1} ($P_{d.max}$). Interestingly in 17 m $NaClO_4$ electrolyte, PEDOT-tos exhibited very high $E_{d.max.}$ and $P_{d.max.}$ of around 14 Wh kg^{-1} (at P_d = 120 W kg^{-1}) and 7210 W kg^{-1} (at E_d = 5 Wh kg^{-1}), respectively (Fig. 6a). Here reported $E_{d.max}$ and $P_{d.max}$ values are among highest reported values for PEDOT-tos supercapacitors (Table S2). Presumably, the wide ESW of WiSE granted the fullest use of charge storage sites of

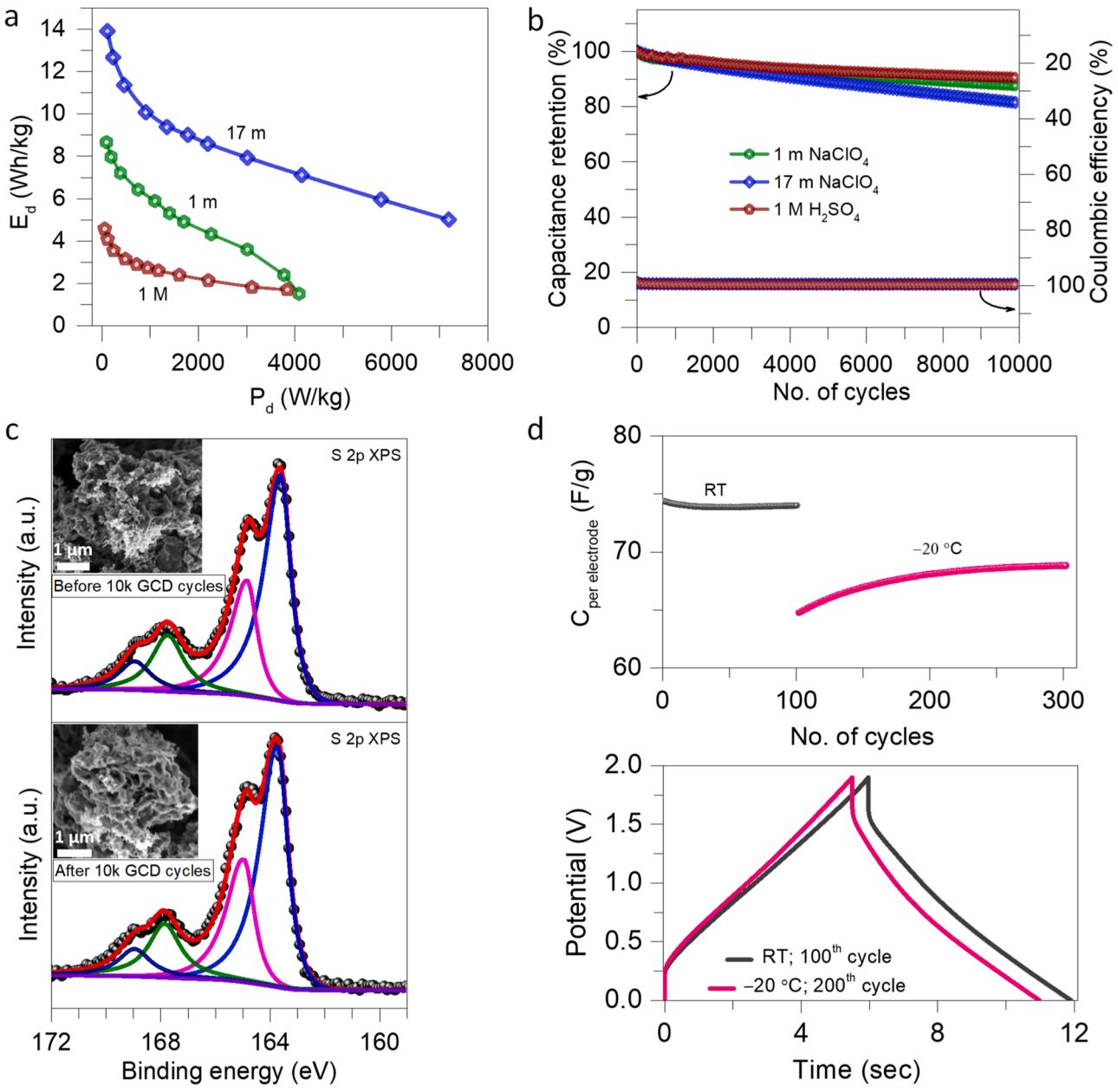

Fig. 6. (a) Ragone plot and (b) Galvanostatic charge-discharge (at $J = 10$ A g^{-1}) stability cycles of PEDOT-tos supercapacitors in 1 M H_2SO_4, 1 m $NaClO_4$, and 17 m $NaClO_4$ electrolytes, (c) S 2p XPS of PEDOT-tos electrode before and after 10,000 cycles. Inset: SEM images of electrode material electrode before and after 10,000 cycles, and (d) Performance comparison of PEDOT-tos supercapacitor at RT and –20 °C; upper panel: number of cycles, lower panel: GCD after 100th cycle at RT and 200th cycle at –20 °C at a J of 10 A g^{-1}.

PEDOT-tos, which were otherwise inaccessible in narrower ESW of dilute aqueous electrolytes. The long-life stability of PEDOT supercapacitor was evaluated by performing 10,000 continuous GCD cycles at a J of 10 A g^{-1}. Notably, PEDOT-tos supercapacitor retained >80 % of its capacitance value in all three electrolytes – 1 M H_2SO_4, 1 m $NaClO_4$, and 17 m $NaClO_4$. Additionally, ~100 % Coulombic efficiency suggested a facile charge-percolation throughout the GCD cycles [44]. To ensure the stability of PEDOT backbone and tosylate after 10,000 continuous GCD cycles in 17 m $NaClO_4$ WiSE, XPS and SEM analyses of the electrode material were performed (Fig. 6c). Before and after 10,000 cycles, the electrode materials were peeled off from the graphite sheets, washed with water and ethanol, and dried in a vacuum oven. In both cases, the S 2p XPS spectra showed two doublet peaks at around 163.7 eV and 167.8 eV binding energies, corresponding to S $2p_{3/2}$ of PEDOT and tosylate, respectively (Fig. 6c) [37]. This suggests that the tosylate remained intact with PEDOT and was not replaced by perchlorate during the electrochemical measurements. Traces of unwashed nafion and perchlorate were observed in the XPS analysis after 10,000 GCD cycles (Fig. S13). The lettuce coral-like structure of PEDOT-tos remained unchanged even after 10,000 GCD cycles (Fig. 6c, insets). To demonstrate the temperature-dependent stability of our PEDOT-tos supercapacitor, 200 continuous GCD cycles were performed at –20 °C. The results showed only a 6–10 F decrease in capacitance at –20 °C compared to room temperature (RT), highlighting the importance of using the highly conductive 17 m $NaClO_4$ WiSE with a low freezing point (Fig. 6d).

To test the performance of our PEDOT-tos supercapacitor beyond 1.9 V ESW, we increased the potential window to 2.2 V in a 17 m $NaClO_4$ WiSE. Electrochemical, spectroscopy, and microscopy characterizations are provided in the supporting information (Fig. S14 and S15). The CV showed a resistive nature after a 1.9 V potential, which was also

reflected in the GCD curve with a large IR drop (Fig. S14c, d). The $C_{gr.}$, $E_{d.max.}$, and $P_{d.max.}$ of the PEDOT-tos supercapacitor were 112.7 F g^{-1}, 17.3 Wh kg^{-1}, and 8000 W kg^{-1}, respectively (Fig. S14e, f). Interestingly, the PEDOT-tos supercapacitor showed >85 % capacitance retention after 10,000 continuous GCD cycles (at J = 10 A g^{-1}) with ~100 % Coulombic efficiency (Fig. S15a). The S 2p XPS and SEM revealed the intact chemical nature and morphology of our PEDOT-tos electrode material even after 10,000 GCD cycles in a 2.2 V potential window (Fig. S15b, c). These results suggest that our material can sustain a high ESW of 2.2 V, however, the energy storage contribution with respect to 1.9 V ESW was not significantly high.

4. Conclusions

We have synthesized thin sheets of PEDOT-tos by an oxidative chemical polymerization approach. Further careful characterizations demonstrated the lettuce coral-like structure of highly conducting (σ = 3500 S m^{-1}) PEDOT-tos. The supercapacitive performance of our PEDOT-tos was evaluated in three different electrolytes – aqueous 1 M H_2SO_4, 1 m $NaClO_4$, and 17 m $NaClO_4$ WiSE. PEDOT-tos supercapacitors have underperformed (E_d = 4.5 Wh kg^{-1}) in aqueous H_2SO_4 electrolyte, due to the narrow electrochemical stability window (ESW = 1 V). Interestingly, for PEDOT-tos supercapacitor, we have achieved an ESW of 1.9 V in 17 m $NaClO_4$ WiSE. This increased the E_d of PEDOT-tos supercapacitor by 3-times compared to 1 M H_2SO_4 electrolyte. The maximum E_d and P_d of PEDOT-tos supercapacitor were calculated around 14 Wh kg^{-1} and 7210 W kg^{-1}, respectively, with >80 % capacitance retention over 10,000 continuous GCD cycles. Raman spectra of PEDOT-tos electrode showed different doping-state and stable backbone of PEDOT-tos at 0, 0.5, 1, 1.5, 1.9 V potentials. We have measured the density, viscosity, Raman spectroscopy, and NMR spectroscopy of $NaClO_4$ WiSE for its unique solvation chemistry. Our PEDOT-tos supercapacitor showed minor capacitance change when measured at –20 °C temperature. Also, PEDOT-tos supercapacitor showed high energy and power densities and >85 % GCD stability in a 2.2 V potential window. To the best of our knowledge this is the widest ESW achieved for a PEDOT-tos supercapacitor in an aqueous-based electrolyte (Tables S1 and S2). We highly recommend WiSE for PEDOT-based supercapacitors.

CRediT authorship contribution statement

Plawan Kumar Jha: Writing – original draft, Visualization, Methodology, Investigation, Formal analysis, Conceptualization. **Sachin Kochrekar:** Investigation, Formal analysis. **Ashwini Jadhav:** Writing – review & editing, Formal analysis. **Robert Lassfolk:** Formal analysis. **Mikko Salomäki:** Formal analysis. **Ermei Mäkilä:** Formal analysis. **Carita Kvarnström:** Writing – review & editing, Supervision, Resources, Project administration.

Declaration of competing interest

The authors declare that they have no known competing financial interests or personal relationships that could have appeared to influence the work reported in this paper.

Acknowledgements

P.K.J., S.K., and A.J. acknowledge the Real Estate Foundation, Finland, and Business Finland (COMPOL project) for their financial support. P.K.J. and R.L. are grateful to the Turku Center for Chemical and Molecular Analytics (CCMA) for providing the NMR facility. P.K.J. thanks Pooja Sindhu from IISER Pune for the TEM images. P.K.J. thanks Pia Damlin from university of Turku for the technical help.

Supplementary materials

Supplementary material associated with this article can be found, in the online version, at doi:10.1016/j.ensm.2024.103758.

References

[1] P. Simon, Y. Gogotsi, Perspectives for electrochemical capacitors and related devices, Nat. mater. 19 (2020) 1151–1163.
[2] J. Yu, C. Mu, X. Qin, C. Shen, B. Yan, H. Xue, H. Pang, Development of high-voltage aqueous electrochemical energy storage devices, Adv. Mater. Interfaces 4 (2017) 1700279.
[3] C. Zhao, W. Zheng, A review for aqueous electrochemical supercapacitors, Front. Energy Res. 3 (2015) 23.
[4] B. Pal, S. Yang, S. Ramesh, V. Thangadurai, R. Jose, Electrolyte selection for supercapacitive devices: a critical review, Nanoscale Adv 1 (2019) 3807–3835.
[5] C. Zhong, Y. Deng, W. Hu, J. Qiao, L. Zhang, J. Zhang, A review of electrolyte materials and compositions for electrochemical supercapacitors, Chem. Soc. Rev. 44 (2015) 7484–7539.
[6] L. Suo, O. Borodin, T. Gao, M. Olguin, J. Ho, X. Fan, C. Luo, C. Wang, K. Xu, Water-in-salt" electrolyte enables high-voltage aqueous lithium-ion chemistries, Science 350 (2015) 938–943.
[7] J. Han, A. Mariani, S. Passerini, A. Varzi, A perspective on the role of anions in highly concentrated aqueous electrolytes, Energy Environ. Sci. 16 (2023) 1480–1501.
[8] X. Tian, Q. Zhu, B. Xu, Water-in-Salt" Electrolytes for Supercapacitors: a Review, ChemSusChem 14 (2021) 2501–2515.
[9] L. Suo, D. Oh, Y. Lin, Z. Zhuo, O. Borodin, T. Gao, F. Wang, A. Kushima, Z. Wang, H.-C. Kim, Y. Qi, W. Yang, F. Pan, J. Li, K. Xu, C. Wang, How solid-electrolyte interphase forms in aqueous electrolytes, J. Am. Chem. Soc. 139 (2017) 18670–18680.
[10] Y. Sui, A. Scida, B. Li, C. Chen, Y. Fu, Y. Fang, P.A. Greaney, T. Osborn Popp, D.-e. Jiang, C. Fang, X. Ji, The Influence of Ions on the Electrochemical Stability of Aqueous Electrolytes, Angew. Chem. Int. Ed. (2024) e202401555.
[11] L. Suo, O. Borodin, Y. Wang, X. Rong, W. Sun, X. Fan, S. Xu, M.A. Schroeder, A. V. Cresce, F. Wang, C. Yang, Y.-S. Hu, K. Xu, C. Wang, Water-in-salt" electrolyte makes aqueous sodium-ion battery safe, green, and long-lasting, Adv. Energy Mater. 7 (2017) 1701189.
[12] D.P. Leonard, Z. Wei, G. Chen, F. Du, X. Ji, Water-in-salt electrolyte for potassium-ion batteries, ACS Energy Lett 3 (2018) 373–374.
[13] L. Jiang, L. Liu, J. Yue, Q. Zhang, A. Zhou, O. Borodin, L. Suo, H. Li, L. Chen, K. Xu, Y.-S. Hu, High-voltage aqueous Na-ion battery enabled by inert-cation-assisted water-in-salt electrolyte, Adv. Mater. 32 (2020) 1904427.
[14] B.J. Choudhury, K. Ingtipi, V.S. Moholkar, Improved energy density of reduced graphene oxide based aqueous symmetric supercapacitors in redox-active and "water-in-salt" electrolytes, J. Energy Storage 52 (2022) 105006.
[15] M.H. Lee, S.J. Kim, D. Chang, J. Kim, S. Moon, K. Oh, K.-Y. Park, W.M. Seong, H. Park, G. Kwon, B. Lee, K. Kang, Toward a low-cost high-voltage sodium aqueous rechargeable battery, Mater. Today 29 (2019) 26–36.
[16] J. Park, J. Lee, W. Kim, Redox-active water-in-salt electrolyte for high-energy-density supercapacitors, ACS Energy Lett 7 (2022) 1266–1273.
[17] J. Park, J. Lee, W. Kim, Water-in-salt electrolyte enables ultrafast supercapacitors for AC line filtering, ACS Energy Lett 6 (2021) 769–777.
[18] R. Yewale, P. Damlin, M. Salomäki, C. Kvarnström, Layer-by-layer approach to engineer and control conductivity of atmospheric pressure vapor phase polymerized PEDOT thin films, Mater. Today Commun. 25 (2020) 101398.
[19] S. Maity, S. Datta, M. Mishra, S. Banerjee, S. Das, K. Chatterjee, Poly(3,4-ethylenedioxythiophene)-tosylate—Its synthesis, properties and various applications, Polym. Adv. Technol. 32 (2021) 1409–1427.
[20] J.M. D'Arcy, M.F. El-Kady, P.P. Khine, L. Zhang, S.H. Lee, N.R. Davis, D.S. Liu, M. T. Yeung, S.Y. Kim, C.L. Turner, A.T. Lech, P.T. Hammond, R.B. Kaner, Vapor-phase polymerization of nanofibrillar poly(3,4-ethylenedioxythiophene) for supercapacitors, ACS Nano 8 (2014) 1500–1510.
[21] L. Groenendaal, F. Jonas, D. Freitag, H. Pielartzik, J.R. Reynolds, Poly(3,4-ethylenedioxythiophene) and its derivatives: past, present, and future, Adv. Mater. 12 (2000) 481–494.
[22] S. Suh, K. Kim, J. Park, W. Kim, Ultrafast flexible PEDOT: PSS supercapacitor with outstanding volumetric capacitance for AC line filtering, Chem. Eng. J. 463 (2023) 142377.
[23] M.F. Jimoh, M.F. El-Kady, G.S. Carson, M.B. Anderson, Q. Duong, R.B. Kaner, Template-free route to PEDOT nanofibers for 3D electrodes with ultrahigh capacitance and excellent cycling stability, Energy Storage Mater. 61 (2023) 102850.
[24] X. Han, J. Sun, Q. Li, X. He, L. Dang, Z. Liu, Z. Lei, Highly flexible PEDOT film assembled with solution-processed nanowires for high-rate and long-life solid-state supercapacitors, ACS Sustain. Chem. Eng. 11 (2023) 2938–2948.
[25] M. Rajesh, C.J. Raj, R. Manikandan, B.C. Kim, S.Y. Park, K.H. Yu, A high performance PEDOT/PEDOT symmetric supercapacitor by facile in-situ hydrothermal polymerization of PEDOT nanostructures on flexible carbon fibre cloth electrodes, Mater. Today Energy 6 (2017) 96–104.
[26] Z. Su, C. Yang, C. Xu, H. Wu, Z. Zhang, T. Liu, C. Zhang, Q. Yang, B. Li, F. Kang, Co-electro-deposition of the MnO_2–PEDOT:PSS nanostructured composite for high areal mass, flexible asymmetric supercapacitor devices, J. Mater. Chem. A 1 (2013) 12432–12440.

[27] X. Wang, A. Abdurexit, R. Jamal, T. Abdiryim, N. Fan, Y. Liu, K. Song, H. Yang, Preparation of PEDOT/$Ti_3C_2T_x$/Co_3S_2 composite for quasi−solid−state hybrid supercapacitor with enhanced electrochemical performance, J. Alloys Compd. 980 (2024) 173609.
[28] R. Liu, J. Duay, S.B. Lee, Redox exchange induced MnO_2 nanoparticle enrichment in poly(3,4-ethylenedioxythiophene) nanowires for electrochemical energy storage, ACS Nano 4 (2010) 4299–4307.
[29] Ö. Yağci, M.B. Arvas, S.A. Yüksel, The effect of zinc and sodium borate doping on the structural, morphological, optical, electrical and electrochemical properties of PEDOT:PSS thin film electrodes for flexible and transparent supercapacitor applications, New J. Chem. (2024) 4096–4108.
[30] L. Manjakkal, A. Pullanchiyodan, N. Yogeswaran, E.S. Hosseini, R. Dahiya, A wearable supercapacitor based on conductive PEDOT: PSS-coated cloth and a sweat electrolyte, Adv. Mater. 32 (2020) 1907254.
[31] D.C. Martin, J. Wu, C.M. Shaw, Z. King, S.A. Spanninga, S. Richardson-Burns, J. Hendricks, J. Yang, The morphology of poly (3, 4-ethylenedioxythiophene), Polym. Rev. 50 (2010) 340–384.
[32] M.N. Gueye, A. Carella, J. Faure-Vincent, R. Demadrille, J.-P. Simonato, Progress in understanding structure and transport properties of PEDOT-based materials: a critical review, Prog. Mater. Sci. 108 (2020) 100616.
[33] A.V. Volkov, K. Wijeratne, E. Mitraka, U. Ail, D. Zhao, K. Tybrandt, J. W. Andreasen, M. Berggren, X. Crispin, I.V. Zozoulenko, Understanding the Capacitance of PEDOT: PSS, Adv. Funct. Mater. 27 (2017) 1700329.
[34] I. Zozoulenko, J.F. Franco-Gonzalez, V. Gueskine, A. Mehandzhiyski, M. Modarresi, N. Rolland, K. Tybrandt, Electronic, optical, morphological, transport, and electrochemical properties of PEDOT: a theoretical perspective, Macromolecules 54 (2021) 5915–5934.
[35] W.W. Chiu, J. Travaš-Sejdić, R.P. Cooney, G.A. Bowmaker, Studies of dopant effects in poly(3,4-ethylenedi-oxythiophene) using Raman spectroscopy, J. Raman Spectrosc. 37 (2006) 1354–1361.
[36] K. Aasmundtveit, E. Samuelsen, L. Pettersson, O. Inganäs, T. Johansson, R. Feidenhans, Structure of thin films of poly (3, 4-ethylenedioxythiophene), Synth. Met. 101 (1999) 561–564.
[37] G. Zotti, S. Zecchin, G. Schiavon, F. Louwet, L. Groenendaal, X. Crispin, W. Osikowicz, W. Salaneck, M. Fahlman, Electrochemical and XPS studies toward the role of monomeric and polymeric sulfonate counterions in the synthesis, composition, and properties of poly(3,4-ethylenedioxythiophene), Macromolecules 36 (2003) 3337–3344.
[38] A.N. Fuentes, J.M. Casas, Thermochemical and ionic speciation modeling of the aqueous sulfuric acid system Up to 6 molal and 0–100 °C, J. Solution Chem. 52 (2023) 1176–1193.
[39] A.G. Miller, J.W. Macklin, Vibrational spectroscopic studies of sodium perchlorate contact ion pair formation in aqueous solution, J. Phys. Chem. 89 (1985) 1193–1201.
[40] G.J. Templeman, A.L. Van Geet, Sodium magnetic resonance of aqueous salt solutions, J. Am. Chem. Soc. 94 (1972) 5578–5582.
[41] M.S. Greenberg, A.I. Popov, Spectroscopic studies of ionic solvation. XXI. A raman, infrared, and NMR study of sodium perchlorate solutions in nonaqueous solvents, J. Solut. Chem. 5 (1976) 653–665.
[42] X. Bu, L. Su, Q. Dou, S. Lei, X. Yan, A low-cost “water-in-salt” electrolyte for a 2.3 V high-rate carbon-based supercapacitor, J. Mater. Chem. A 7 (2019) 7541–7547.
[43] Y.-H. Zhang, C.K. Chan, Observations of water monomers in supersaturated NaClO4, LiClO4, and Mg (ClO4)2 droplets using Raman spectroscopy, J. Phys. Chem. A 107 (2003) 5956–5962.
[44] P.K. Jha, S.K. Singh, V. Kumar, S. Rana, S. Kurungot, N. Ballav, High-level supercapacitive performance of chemically reduced graphene oxide, Chem 3 (2017) 846–860.
[45] P.K. Jha, K. Gupta, A.K. Debnath, S. Rana, R. Sharma, N. Ballav, 3D mesoporous reduced graphene oxide with remarkable supercapacitive performance, Carbon N Y 148 (2019) 354–360.
[46] W. Zheng, J. Halim, J. Rosen, M.W. Barsoum, Aqueous electrolytes, MXene-based supercapacitors and their self-discharge, Adv. Energy Sustainability Res. 3 (2022) 2100147.
[47] B.E. Conway, Electrochemical supercapacitors: Scientific Fundamentals and Technological Applications, Springer Science & Business Media, 2013.
[48] J. Wang, J. Polleux, J. Lim, B. Dunn, Pseudocapacitive contributions to electrochemical energy storage in TiO2 (anatase) nanoparticles, J. Phys. Chem. C 111 (2007) 14925–14931.
[49] A. Jadhav, P.K. Jha, M. Salomäki, S. Granroth, P. Damlin, C. Kvarnström, Supercapacitive performance of ionic-liquid-intercalated two-dimensional $Ti_3C_2T_x$ in redox electrolyte, Cell Rep. Phys. Sci. 5 (2024) 101788.